Hydraulic Fracturing Mechanism in Reservoirs with a Linear Inclusion Fissure

Wang Wenwu[1, 2], Zhu Xiuxing[1], Ye Guigen[1], Han Zhongying[1] & Xue Shifeng[1*]

[1]Department of Engineering Mechanics, College of Pipeline and Civil Engineering, China University of Petroleum, Shandong, 266580, China
[2]PetroChina Changqing Oilfield Company Machinery Manufacturing Factory, Shanxi, 710201, China
E-mail: sfeng@upc.edu.cn

Abstract. Hydraulic fracturing technology is widely used in most oil-water wells to improve production. However, the mechanism of fracturing in a reservoir with inclusion fissures is still unclear. In this study, a theoretical model was developed to determine the stress distribution during hydraulic fracturing. The line inclusion fissure was regarded as a thin bar and the stress around the artificial fracture, which is affected by a single line inclusion, was determined using the Eshelby equivalent inclusion theory. Stress intensity factors at the tip of both the artificial fracture and the inclusion were achieved, and initiation of the fracture was predicted. Furthermore, to validate the theoretical model, re-fracturing experiments were performed on a large-scale tri-axial system. The results showed that the defects reduce the intensity of the rock, which introduces the possibility that more complex fractures emerge in the reservoir. The results also showed that the fracture direction is governed by far-field stress. The obtained conclusions are helpful to better understand the mechanism of hydraulic fracturing in reservoirs.

Keywords: *hydraulic fracturing; large-scale simple; reservoir with inclusion fissure; stress evolution; tri-axial simulation.*

1 Introduction

Hydraulic fracturing is an important enhanced oil recovery technology for low permeability reservoirs, which occupy a considerable proportion of oil reserves [1,2]. Once hydraulic fracturing fails, re-fracturing will be used in most oil-water wells. As an enhanced recovery technique, re-fracturing technology was first developed in the 1950s and it has become one of the most important methods to improve the production of oil and gas fields. Understanding the initiation and propagation of new cracks in re-fracturing is of significant importance. However, in spite of extensive studies, the fundamental mechanism of re-fracturing is still poorly understood, which hinders the development of re-fracturing technology.

Received January 13th, 2016, Revised March 21st, 2016, Accepted for publication April 12th, 2016.
 ISSN: 2337-5779, DOI: 10.5614/j.eng.technol.sci.2016.48.2.8

Numerous studies have been carried out to explore the mechanism of hydraulic fracturing, mainly focusing on the interactions between artificial and natural fractures in naturally fractured reservoirs [3,4]. Experiments have showed that – because of the complex influences of various factors, such as far-field stress, loading pressure and inclusions – a reservoir may present different fracture mechanisms or patterns [5-9]. The influences of stress state, hydraulic injection rate and the conductivity of pre-existing fractures on the re-fracturing mechanism have been widely studied [10].

Liu, *et al.* [8] designed a new experimental model to simulate the influence of a natural fracture network on the propagation geometry of hydraulic fractures in naturally fractured formations by using a tri-axial fracturing system. They stated that the principle of hydraulic fracture propagation is that it follows the least resistance, the most preferential propagation, and the shortest propagation paths. Xu, *et al.* [11] studied the fracture pattern of hydraulic fracturing under various radial boundary and fluid injection rates. They showed that the fracture patterns of hydraulic fracturing in clay greatly depends on the size of radial boundary and fluid injection rate, and that the fracturing orientation induced by hydraulic fracturing can be controlled by changing the size of the radial boundary and fluid injection rate. Huang, *et al.* [12] studied the initiation pressure, location, and orientation of hydraulic fractures. They pointed out that the axial stress is not a good predictor of transverse fracture initiation. They presented special cases in which the highest tensile principal stress reached the tensile strength of the rock simultaneously at all points on the circumference of the wellbore. Transverse fractures are proposed to be initiated in those cases. Jin Yan, *et al.* [13] analyzed the effects of salutatory barriers on hydraulic fracture propagation, but no further results were presented. Recently, numerical methods have been widely used to solve the hydraulic fracture problem and many related studies can be found in the literature [14-16].

These pioneering works provide important clues to the study of the mechanism of re-fracturing. During re-fracturing, the onset and propagation of new cracks are significantly affected by the structural characteristics of the reservoir. More importantly, numerous types of complex-isolated inclusions are present in the reservoirs. Thus, the stress singularity always exists at the tip of the flake inclusions, thereby generating micro-cracks [17]. All these factors make the problem much more complex and hence the mechanism of the re-fracturing remains unclear.

The remainder of this paper is organized as follows: Section 2 first describes the theoretical model that was developed to solve the re-fracturing problem in a reservoir with line inclusions. Section 2 then presents the stress intensity factors at the tip of both the artificial fracture and the inclusion, which can be used to

predict the initiation of fracture. Finally, an improved large-scale tri-axial experimental system is also presented in Section 2 and the re-fracturing experiments are described. Section 3 presents the re-fracturing results for five typical cases and the re-fracturing mechanisms are discussed in this section as well. The conclusions are summarized in Section 4.

2 Materials and Methods

2.1 Theoretical Analysis

The theoretical model of the stress distribution in a reservoir with a line inclusion before re-fracturing is schematically presented in Figure 1.

The length of the inclusion is assumed to be much larger than its width; thus, the inclusion can be regarded as a straight line. The global coordinate system (x, y) is attached to the artificial fracture. Coordinates x and y are parallel and normal to the direction of maximum stress, respectively. A local coordinate system (x', y') is attached to the inclusion. Coordinates x' and y' are parallel and normal to the direction of the inclusion, respectively.

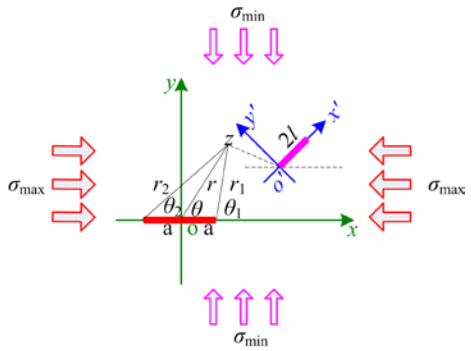

Figure 1 Stress distribution in a reservoir with linear inclusion before re-fracturing.

In this work, only the elastic deformation was considered for the inclusion body. Therefore, the inclusion could be further treated as a thin bar to reflect the discontinuity of the stress between the inclusion and the rock matrix. Moreover, the Eshelby equivalent inclusion theory was adopted to solve the problem and only the rock skeleton stress was considered.

The stress in the reservoir with a line inclusion resulted from the following three parts:

1. Stress induced by the artificial fracture;
2. Stress induced by the line inclusion;
3. Far-field stress.

Thus, the total stress in the reservoir can be given in Eq. (1) as follows:

$$\sigma_{ij}(x,y)=\sigma_{\mathrm{a},ij}(x,y)+\sigma_{\mathrm{d},ij}(x,y)+\sigma_{\mathrm{w},ij}(x,y)\qquad (i,j)=(x,y) \tag{1}$$

where $\sigma_{ij}(x,y)$ is the total stress, $\sigma_{\mathrm{a},ij}(x,y)$ is the stress induced by the artificial fracture, $\sigma_{\mathrm{d},ij}(x,y)$ is the stress induced by the line inclusion, and $\sigma_{\mathrm{w},ij}(x,y)$ is the far-field stress.

The boundary conditions are given as follows:

1. Total stress at the edge of the line inclusion should meet the displacement compatibility relations. It can be given in terms of the local coordinate $x'o'y'$ as

$$\begin{aligned}
&\frac{\partial u'_{\mathrm{a}}(x',+0)}{\partial x'}+\frac{\partial u'_{\mathrm{d}}(x',+0)}{\partial x'}+\frac{\partial u'_{\mathrm{w}}(x',+0)}{\partial x'}=\frac{\partial u_{\mathrm{d}}{}^{*}(x')}{\partial x'} \quad (0\le x'\le 2l)\\
&\frac{\partial v'_{\mathrm{a}}(x',+0)}{\partial x'}+\frac{\partial v'_{\mathrm{d}}(x',+0)}{\partial x'}+\frac{\partial v'_{\mathrm{w}}(x',+0)}{\partial x'}=\frac{\partial v_{\mathrm{d}}{}^{*}(x')}{\partial x'} \quad (0\le x'\le 2l)
\end{aligned} \tag{2}$$

   where u' and v' are the displacement component along the x' direction and the y' direction, respectively. The subscripts a, d, and w reflect the displacements caused by the artificial fracture, the line inclusion and the far-field stress, respectively. The asterisk represents the final displacement at the edge of the inclusion.

2. The artificial fracture is only subjected to a tensile stress p on its surface, with a direction perpendicular to the fracture surface. Therefore, we have

$$\sigma_{\mathrm{a},yy}(x,0)+\sigma_{\mathrm{d},yy}(x,0)+\sigma_{\mathrm{w},yy}(x,0)=p,\quad (-a=<x<=a) \tag{3}$$

$$\sigma_{\mathrm{a},xy}(x,0)+\sigma_{\mathrm{d},xy}(x,0)+\sigma_{\mathrm{w},xy}(x,0)=0,\quad (-a=<x<=a) \tag{4}$$

   Solving Eqs. (2), (3) and (4) obtains four Cauchy singular integral equations. Thus, the interaction problem between the single line inclusion and the artificial fracture becomes basically algebraic in nature and can be investigated by using the four Cauchy singular integral equations. The stress at any point of the reservoirs can be determined by using these four Cauchy singular integral equations. In this way, the stress intensity factor at the tip of the artificial fracture and inclusion can be achieved.

If the artificial fracture and line inclusion are disjoint, then the stress intensity factor at the tip of the artificial fracture can be given by Eqs. (5) and (6).

$$K_{\mathrm{I}}(-a)=\frac{2\mu}{\kappa+1}\lim_{x\to -a}\sqrt{2(a+x)}g(x) \tag{5}$$

$$K_{\mathrm{I}}(a)=-\frac{2\mu}{1+\kappa}\lim_{x\to a}\sqrt{2(a-x)}g(x) \tag{6}$$

where a is the half-length of artificial fracture, K_{I} is the stress intensity factor of model I crack, and κ is the elastic constant of the rock matrix, which can be given as $\kappa=3-4\upsilon$ for the plane strain problem, where υ is the Poisson ratio. $g(x)$ is the dislocation density function of the artificial fracture at $y = 0$ ($x=-a\sim+a$), which can be presented in Eq. (7) as follows:

$$g(x)=\frac{\partial}{\partial x}\left[u_y(x,+0)-u_y(x,-0)\right] \quad (-a<x<a) \tag{7}$$

The stress intensity factor at the tip of the line inclusion can be expressed by using the local coordinate system, i.e.

$$K'_{\mathrm{I}}(0)=-\frac{\kappa-1}{2(\kappa+1)}\lim_{x'\to 0}\sqrt{2x'}q(x') \tag{8}$$

$$K'_{\mathrm{I}}(2l)=\frac{\kappa-1}{2(\kappa+1)}\lim_{x'\to 2l}\sqrt{2(2l-x')}q(x') \tag{9}$$

where $2l$ is the length of the inclusion and $q(x')$ is the tangential constraint stress loaded on the rock matrix by the inclusion, which is given by

$$q(x')=\sigma_{xy}(x',-0)-\sigma_{xy}(x',+0) \tag{10}$$

Consequently, whether or not the crack can propagate along the fracture or the inclusion can be determined by comparing the theoretical result with the critical stress intensity factor, K_{IC}, of the rock matrix.

Eqs. (8), (9) and (10) show that the stress intensity factor at the tip of the line inclusion is affected by the local stress around the inclusion. A detail that should be pointed out is that the local stress around the inclusion is dominated by the far-field stress and the pressure located on the inner boundary of the artificial fracture. When the far-field stress and the pressure on the inner boundary reach critical values, K'_{I} becomes larger than K_{IC}. Thus, new cracks emerge along the defect. In the following paragraphs, our re-fracturing experiments will be reported to show the propagations of the cracks that initiate from both the artificial fracture and the inclusions.

2.2 Experimental Procedure

Re-fracturing experiments were performed on an improved large-scale tri-axial rock mechanics experimental system. The tri-axial rock mechanics experimental system contained a hydraulic pump, water station, control cabinet, operating system and a high-pressure cylinder. The hydraulic pump and high-pressure cylinder are shown in Figure 2. The maximum loading pressure of this experimental system could reach 30 MPa, the inner diameter was 800 mm.

(a) (b)

Figure 2 (a) Hydraulic pump and (b) high-pressure cylinder.

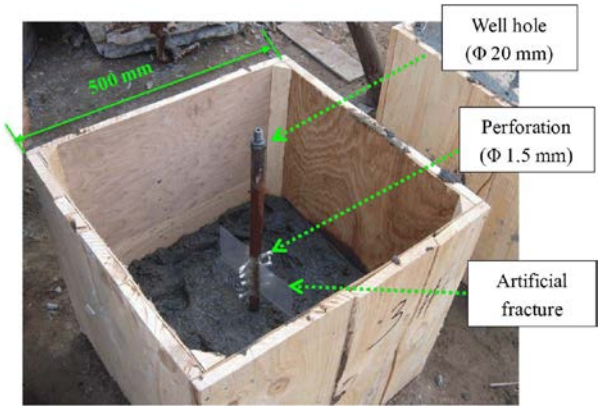

Figure 3 Inner structure of the cubic sample.

Cubic blocks measuring 500 mm on each side were prepared with cement concrete. The well hole was positioned in the middle of the cubic sample and

had a diameter of 20 mm. Eight perforations with a diameter of 1.5 mm were located near the bottom of the sample. Random defects were added in the samples and the initial artificial fracture was simulated by a thin plastic sheet, as shown in Figure 3.

The cubic samples were positioned in the high-pressure cylinder, which is one of the most important pieces of equipment of the entire experimental system. In-situ stress conditions were further performed on the sample. Then, re-fracturing was carried out. The sample was subjected to hydrodynamic pressure and compression along three different directions.

Table 1 Loading far-field stress conditions.

Sample Number	Experimental Conditions	First Fracturing (MPa)			Second Fracturing (MPa)		
		σ_x	σ_y	σ_z	σ_x	σ_y	σ_z
1#	with no artificial fracture and inclusions	0	0	0			
2#	only with inclusions	3	3	3	3	4	5
3#	only with artificial fracture	2	3	4	3	2	4
4#	with both artificial fracture and inclusions	4	4	4	1	2	3
6#	with both artificial fracture and inclusions	3	4	5	3	4	5

To investigate the initiation and propagation of the cracks during re-fracturing, we discuss five typical cases. The loads in the five cases are shown in Table 1. Here, σ_x reflects the normal stress along the artificial fracture. Before fracturing, the mechanical parameters of the rock matrix were measured on a group of small samples. The measured elastic modulus of the rock matrix was 2.4 GPa and the Poisson's ratio was approximately 0.23.

3 Results and Discussion

After fracturing, the fracture morphologies of the six samples were carefully observed.

No artificial fracture and inclusions existed and no stress was loaded in Case 1. In this case, fracturing was carried out only once. The highest pump pressure was approximately 4.5 MPa. After fracturing, a vertical fracture formed along the well hole, as shown in Figures 4(a) and 4(b).

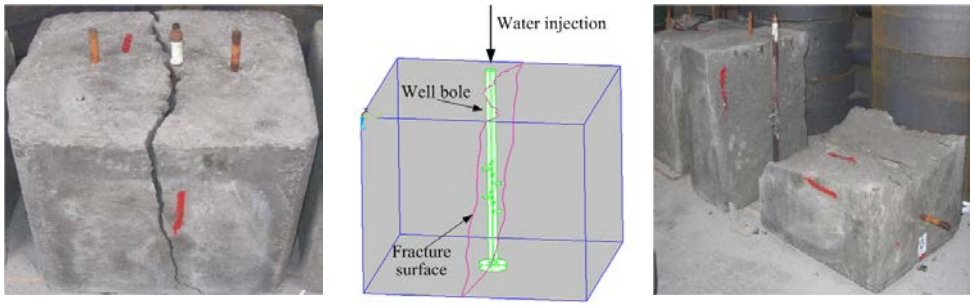

(a) (b) (c)

Figure 4 Fracture morphology of sample #1 after hydraulic fracturing.

In Case 2, random inclusions were set in the sample and the initial stress condition was $(\sigma_x, \sigma_y, \sigma_z) = (3,3,3)$ MPa. During the first fracturing, the hydrostatic pressure was 6.5 MPa. After the first fracturing, a main fracture formed along the horizontal direction in both samples #1 and #2. Then, the loading stress condition was changed to $(\sigma_x, \sigma_y, \sigma_z) = (3,4,5)$ MPa and the second hydraulic fracturing was performed. During the second hydraulic fracturing, the highest pump pressure was reduced to 2.4 MPa because the horizontal crack that formed in the first fracturing reduced the pressure. After the second fracturing, another main crack formed, propagating along the direction of the maximum horizontal principal stress. The fracture morphology of sample #2 after hydraulic fracturing is shown in Figures 5(a) and 5(b). The preset inclusion is clearly evident on the fracture surface (Figure 5(c)), which implies that the crack propagated along the defect during the fracturing.

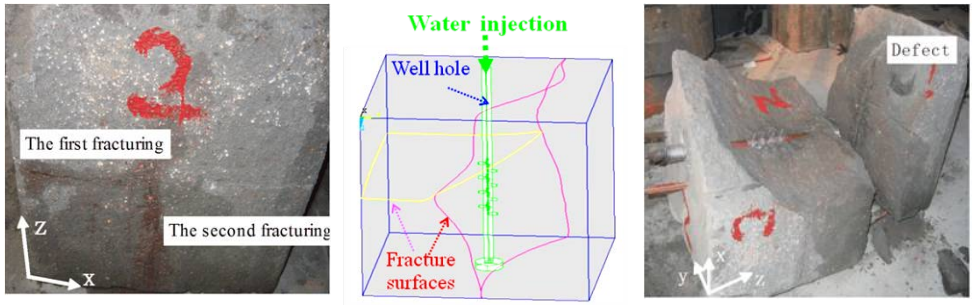

(a) (b) (c)

Figure 5 Fracture morphology of sample #2 after hydraulic fracturing.

Random distributed defects destroy the structural integrity of the rock; thus, the ability of the rock to resist external loading is weakened [13]. When the external loads reach the critical values, the defects will be activated. The activated defects propagate under the external loads, which finally results in rupture of

the sample. Therefore, when the loads reach a certain threshold, random defects are activated in the reservoirs and new fractures form.

Incase 3, an artificial fracture was preset before fracturing and the initial stress condition was $(\sigma_x, \sigma_y, \sigma_z) = (2,3,4)$ MPa. The maximum horizontal principle stress was set to be along the direction of the artificial fracture.

For the first fracturing, the hydrostatic pressure was 6.0 MPa. After the first fracturing, a main fracture formed along the artificial fracture, as shown in Figure 6(a). Then, we changed the direction of the maximum horizontal principal stress to be perpendicular to the artificial fracture and the loading stress condition was changed to $(\sigma_x, \sigma_y, \sigma_z) = (3,4,5)$ MPa. Subsequently, the second hydraulic fracturing was performed. During the second hydraulic fracturing, the highest pump pressure was reduced to 4.2 MPa. Another crack formed in front of the first crack, in the direction of the maximum horizontal principal stress (Figures 6(b) and 6(c)). The first fracture changed the stress condition around the well hole, thereby affecting the initiation of the second crack. When the far-field stress condition is changed, new cracks may emerge under the elicitation effect of the first crack; the propagation direction is controlled by the far-field stress.

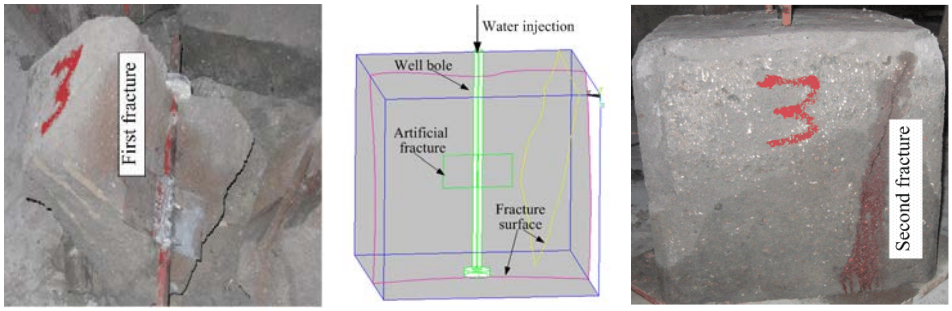

(a) (b) (c)

Figure 6 Fracture morphology of sample #3 after hydraulic fracturing.

In Case 4, both the artificial fracture and inclusions were preset in the sample, and the hydrostatic pressure was increased to 4 MPa. Under such high uniform confining pressure, the artificial fracture closed during the first fracturing. However, a new fracture formed along the direction perpendicular to the fracture. After the first hydraulic fracturing, the loading stress condition was changed to $(\sigma_x, \sigma_y, \sigma_z) = (1,2,3)$ MPa. Then, the second hydraulic fracturing was performed. During the second fracturing, the crack propagated along the crack that formed previously, in the direction of the maximum horizontal

principal stress (Figures 7(a) and 7(b)). More importantly, a preset inclusion was also found on the fracture surface, as shown in Figure 7(c).

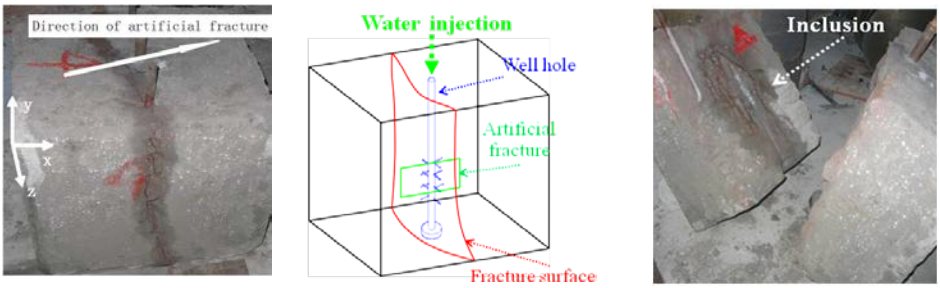

(a) (b) (c)

Figure 7 Fracture morphology of sample #4 after hydraulic fracturing.

In Case 5 (sample #6), the artificial fracture and inclusions were also preset, but the initial stress condition was set to $(\sigma_x, \sigma_y, \sigma_z) = (3,4,5)$ MPa. A fracture formed along the vertical direction during the first fracturing. During the second fracturing, the far-field stress condition remained unchanged and another crack formed along the horizontal direction. Both cracks were not in the direction along the artificial fracture (Figures 8(a) and 8(b)). Similar to Cases 2 and 4, the preset inclusion was also clearly evident on the fracture surface, as shown in Figure 8(a).

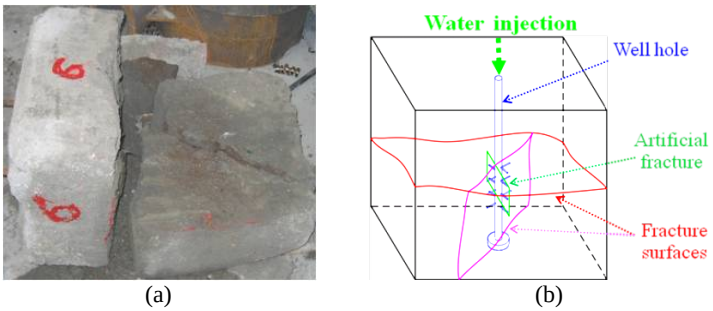

(a) (b)

Figure 8 Fracture morphology of sample #6 after hydraulic fracturing.

Cases 1 to 5 show that the inclusion plays an important role in the propagation of the crack during re-fracturing. When the far-field stress and pump pressure reach critical values, the stress intensity factor at the tip of the inclusion, which can be determined by Eqs. (8) and (9), becomes larger than the critical stress intensity factor of the rock matrix. Thus, a new crack is initiated along the inclusion. The fracture direction is governed by the far-field stress.

We have applied our theoretical method on the Shengli oil fields to predict the direction of the crack propagation after re-fracturing. Before re-fracturing, we predicted the crack propagation direction for well WZ12-1 according to Eqs. (8) and (9), with the predicted direction about NE62°. After re-fracturing, we detected the crack propagation direction for the well by micro seismic monitoring, with the detected direction between NE60°~NE70°, as shown in Figure 9. It was found that the theoretical model showed good agreement with the field-testing result.

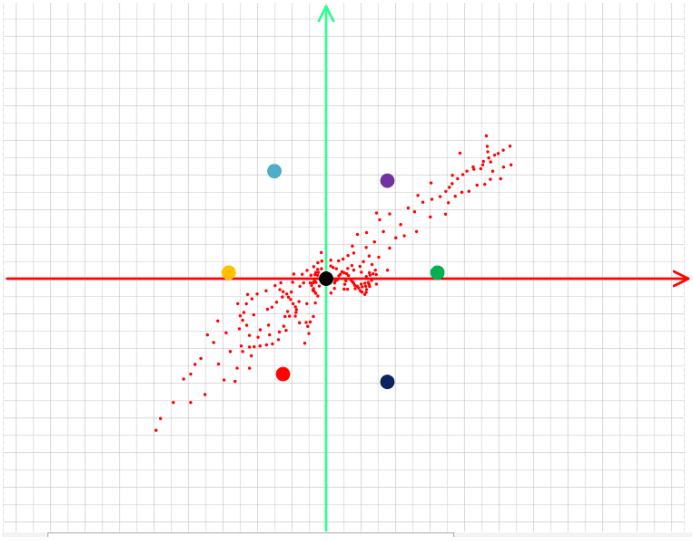

Figure 9 Micro seismic monitoring results for well WZ12-1 (the crack direction is shown by the small dots).

4 Conclusion

Theoretical research and laboratory experiments on the stress distribution during hydraulic fracturing were carried out. The results showed that defects are one of the most important factors that affect crack initiation and propagation on re-fracturing in a reservoir with inclusions. The following conclusions can be drawn:

1. For certain stress conditions, new cracks can form, initiating at the tip of the inclusion.
2. The strength of the rock is weakened by defects in the rock.
3. Whether a new crack can initiate at the inclusion depends on the far-field stress.
4. Under highly uniform confining pressure, the inclusion defect may be the key factor that promotes fracture propagation in the reservoir.

The obtained conclusions are helpful to better understand the mechanism of hydraulic fracturing in reservoirs with inclusion fissures.

Acknowledgements

This study was supported by the National Science and Technology Major Project (grant no. 2011ZX05006-002), the National Nature Science Foundation of China (grant no. 11402278) and the Fundamental Research Funds for the Central Universities.

References

[1] Beugelsdijk, L.J.L., Pater, C.J. & Sato, K., *Experimental Hydraulic Fracture Propagation in a Multi-fractured Medium*, SPE Asia Pacific Conference on Integrated Modelling for Asset Management, 25-26 April, Yokohama, Japan, Society of Petroleum Engineers, SPE 59419, 2000.

[2] Peacock, D.C.P. & Mann, A., *Controls on Fracturing in Carbonate Rocks*, SPE Middle East Oil and Gas Show and Conference, 12-15 March, Kingdom of Bahrain, Society of Petroleum Engineers, SPE 92980, 2005.

[3] Chitrala, Y., Moreno, C., Sondergeld, C. & Rai C., *An Experimental Investigation into Hydraulic Fracture Propagation under Different Applied Stresses in Tight Sands Using Acoustic Emissions*, Journal of Petroleum Science and Engineering, **108**(1), pp. 151-161, 2013.

[4] Nagel, N-B., Sanchez-Nagel, M-A., Zhang, F., Garcia, X. & Lee. B., *Coupled Numerical Evaluations of the Geomechanical Interactions Between a Hydraulic Fracture Stimulation and a Natural Fracture System in Shale Formations*, Rock Mechanics and Rock Engineering, **46**(3), pp. 581-609, 2013.

[5] Bruno, M-S. & Nakagawa. F-M., *Pore Pressure Influence on Tensile Fracture Propagation in Sedimentary Rock*, International Journal of Rock Mechanics and Mining Sciences, **28**(4), pp. 261-273, 1991.

[6] Berchenko, I. & Detournay, E., *Deviation of Hydraulic Fractures Through Poroelastic Stress Changes Induced by Fluid Injection and Pumping*, International Journal of Rock Mechanics and Mining Sciences, **34**(6), pp. 1009-1019, 1997.

[7] Kresse, O., Weng, X., Gu, H. & Wu. R., *Numerical Modeling of Hydraulic Fractures Interaction in Complex Naturally Fractured Formations*, Rock Mechanics and Rock Engineering, **46**(3), pp. 555-568, 2013.

[8] Liu, H., Yang, T., Xu, T. & Yu. Q., *A Comparative Study of Hydraulic Fracturing with Various Boreholes in Coal Seam*, Geosciences Journal, **19**(3), pp. 489-502, 2015.

[9] Zhou, J., Chen, M., Jin, Y. & Zhang. G., *Experimental Study on Propagation Mechanism of Hydraulic Fracture in Naturally Fractured Reservoir*, Acta Petrolei Sinica, **28**(5), pp. 109-113, 2007.

[10] Zhou, J. & Xue, C., *Experimental Investigation of Fracture Interaction between Natural Fractures and Hydraulic Fracture in Naturally Fractured Reservoirs*. SPE EUROPEC/EAGE Annual Conference and Exhibition, 23-26 May, Vienna, Society of Petroleum Engineers, SPE 142890, 2011.

[11] Liu, Z., Chen, M. & Zhang, G., *Analysis of the Influence of a Natural Fracture Network on Hydraulic Fracture Propagation in Carbonate Formations*, Rock Mechanics and Rock Engineering, **47**(2), pp. 575-587, 2014.

[12] Xu, T., Ranjith, P-G., Au, A-S-K., Wasantha, P-L-P., Yang, T-H., Tang, C-A., Liu, H-L. & Chen C-F., *Numerical and Experimental Investigation of Hydraulic Fracturing in Kaolin Clay*, Journal of Petroleum Science and Engineering, **134**(1), pp. 223-236, 2015.

[13] Huang, J., Griffiths, D-V. & Wong. S-W., *Initiation Pressure, Location and Orientation of Hydraulic Fracture*, International Journal of Rock Mechanics and Mining Sciences, **49**(1), pp. 59-67, 2012.

[14] Jin, Y., Chen, M., Zhou, J. & Geng, D., *Experimental Study on the Effects of Salutatory Barrier on Hydraulic Fracture Propagation of Cement Blocks*, Acta Petrolei Sinica, **29**(2), pp. 300-303, 2008.

[15] Carrier, B. & Granet, S., *Numerical Modeling of Hydraulic Fracture Problem in Permeable Medium Using Cohesive Zone Model*, Engineering Fracture Mechanics, **79**(1), pp. 312-328, 2012.

[16] Mohammadnejad, T. & Khoei, A-R., *An Extended Finite Element Method for Hydraulic Fracture Propagation in Deformable Porous Media with The Cohesive Crack Model*, Finite Elements in Analysis and Design, **73**(1), pp. 77-95, 2013.

[17] Peirce, A., *Modeling Multi-scale Processes in Hydraulic Fracture Propagation Using the Implicit Level Set Algorithm*, Computer Methods in Applied Mechanics and Engineering, **283**(1), pp. 881-908, 2015.

[18] Davies, R., Foulger, G., Bindle, A. & Styles, P., *Induced Seismicity and Hydraulic Fracturing for the Recovery of Hydrocarbons*, Marine and Petroleum Geology, **45**(1), pp. 171-185, 2013.